

Fuzzy impedance control of an electro-hydraulic actuator with an extended disturbance observer^{*}

Ming-jie LI¹, Jian-hua WEI¹, Jin-hui FANG^{†‡1}, Wen-zhuo SHI¹, Kai GUO²

¹State Key Laboratory of Fluid Power and Mechatronic Systems, Zhejiang University, Hangzhou 310027, China

²MOE Key Laboratory of High Efficiency and Clean Mechanical Manufacture, Shandong University, Jinan 250061, China

[†]E-mail: jhfang@zju.edu.cn

Received Mar. 14, 2018; Revision accepted May 25, 2018; Crosschecked Sept. 4, 2019

Abstract: In this paper, we deal with both velocity control and force control of a single-rod electro-hydraulic actuator subject to external disturbances and parameter uncertainties. In some implementations, both velocity control and force control are required. Impedance control and an extended disturbance observer are combined to solve this issue. Impedance control is applied to regulate the dynamic relationship between the velocity and output force of the actuator, which can help avoid impact and keep a proper contact force on the environment or workpieces. Parameters of impedance rules are regulated by a fuzzy algorithm. An extended disturbance observer is employed to account for external disturbances and parameter uncertainties to achieve an accurate velocity tracking. A detailed model of load force dynamics is presented for the development of the extended disturbance observer. The stability of the whole system is analyzed. Experimental results demonstrate that the proposed control strategy has not only a high velocity tracking performance, but also a good force adjustment performance, and that it should be widely applied in construction and assembly.

Key words: Fuzzy control; Impedance control; Disturbance observer; Parameter uncertainties; Electro-hydraulic actuator
<https://doi.org/10.1631/FITEE.1800155>

CLC number: TP271.3

1 Introduction


Electro-hydraulic actuators have been widely used in industrial applications and mobile construction vehicles due to their high power-to-mass ratio. High-accuracy velocity tracking is required in some cases, such as hydraulic elevators (Sha et al., 2002; Kim et al., 2005). Sometimes accurate force control is necessary, such as load simulators (Nam, 2001; Truong and Ahn, 2009). Both velocity control and force control are needed in some special applications,

e.g., robot manipulators (Sirouspour and Salcudean, 2001; Zhu and Piedboeuf, 2005) and tunnel boring machines (Yang et al., 2009), in which a dynamic balance between the actuator motion and contact force on the environment or workpieces needs to be maintained.

Raibert and Craig (1981) developed the hybrid position and force control, which divides the control task into position control and force control, but ignores dynamics between the actuator and environment. Impedance control proposed by Hogan (1985a, 1985b, 1985c) solves this problem by regulating dynamic relationship between the end effector position and force as a second-order mass-damper-spring system. Impedance control has been widely used. Fateh (2010) developed a robust impedance control strategy to obtain the desired comfort in a vehicle subjected to road disturbances. Xu (2015) presented a robust impedance control method for high-speed

[‡] Corresponding author

^{*} Project supported by the National Natural Science Foundation of China (No. 51605256), the National High-Tech R&D Program (863) of China (No. 2012AA041803), and the China Postdoctoral Science Foundation (No. 2016M590633)

 ORCID: Jin-hui FANG, <http://orcid.org/0000-0003-4371-2609>

© Zhejiang University and Springer-Verlag GmbH Germany, part of Springer Nature 2019

position and force regulation of a gripper driven by a piezo-electric stack actuator in microassembly. An adaptive impedance control was proposed by Li ZJ et al. (2017) for task- and robot-oriented controls, which helps optimize human-robot cooperative tasks.

High-accuracy motion control is a great challenge for electro-hydraulic systems, due to the parameter uncertainties and uncertain nonlinearities. To obtain a good performance, many control algorithms have been applied. Feedback linearization (Mintsa et al., 2012) uses the pole placement; however, high performance cannot be guaranteed because of the existence of parameter uncertainties and uncertain nonlinearities. Adaptive control (AC) (Ahn et al., 2014) could improve the control system dynamic performance and static precision. However, the disadvantages of AC are that parameters drift and even instability might occur, when encountering disturbances or measurement noises. Unlike AC, sliding mode control (SMC) (Lin et al., 2013; Yu et al., 2017) has been applied to account for system uncertainties and external disturbances. However, chattering in the control signal is inherent in SMC, which could easily excite high frequency modes and degrade the system performance. To overcome the drawbacks of AC and SMC, a new strategy, the adaptive robust control (ARC) method, was proposed (Yao and Tomizuka, 1997; Yao et al., 2000; Chen et al., 2013; Zhang et al., 2016), which effectively integrates the advantages of AC and SMC.

Disturbance compensation is another method used to obtain a good tracking performance. As is not always possible in practice to directly measure disturbance, disturbance observers have been proposed to estimate and compensate for disturbances. A friction observer designed by Friedland and Park (1992) estimated friction and improved the position tracking performance. Chen (2004) developed a nonlinear disturbance observer for disturbances generated by an exogenous system, and global exponential stability was established under certain conditions. Pi and Wang (2010) proposed an observer-based cascade controller for a six-degree-of-freedom (6-DOF) hydraulic manipulator, the effectiveness of which was proved by experiments. A second-order high-pass observer designed by Kim et al. (2013) estimated and compensated for the disturbances in electro-hydraulic actuator position tracking. Simulations and

experiments have demonstrated that the disturbances within bandwidth can be cancelled well. Guo et al. (2015) and Li SZ et al. (2017) used an extended disturbance observer driven by both the state estimation error and the tracking error to estimate not only external disturbances, but also uncertain parameters. Its effectiveness has been validated by experiments. A disturbance observer based adaptive neural network control was proposed for a robotic system (Zhang et al., 2017), which compensated for the model uncertainties, nonlinear dynamics, neural network approximation errors, and external disturbances. A multi-input multi-output (MIMO) extended state observer based integral sliding mode controller (Cui et al., 2017) was developed for an underwater robot. An accurate tracking was achieved through estimating unmeasured velocities, external disturbances, and the upper bound of the uncertainties.

Fuzzy control (Tian et al., 2016; Wei et al., 2016) was a commonly used intelligent control method, which is not based on an accurate mathematical plant model. A unified control strategy of position and force was established by Shibata et al. (1996). Based on parameters of dynamic characteristics of the environment estimated by a linear disturbance observer, force control has been realized via impedance control with fuzzy logic. An adaptive impedance controller based on an evolutionary dynamic recurrent fuzzy neural network (EDRFNN) was developed (Xu et al., 2011), which showed robustness and smoothness in simulations. Therefore, parameters of impedance rules can be regulated by fuzzy algorithms to achieve good performance under gross variations in environmental stiffness (Chen et al., 2005; Fateh and Alavi, 2009).

For hydraulic systems, the existing schemes emphasize only impedance control or high-accuracy position control; however, they could be improved through synthesizing two different strategies. Therefore, a fuzzy impedance controller with an extended disturbance observer based nonlinear velocity controller (FICEDOB) is proposed in this study, combining fuzzy impedance control and extended disturbance observer based nonlinear velocity control (EDOBC). FICEDOB can not only compensate for both external disturbances and parameter uncertainties, but also regulate dynamic relationship between the output force and velocity. Asymptotic velocity

tracking performance can be achieved when the contact force on the environment lies in the allowable range. An expected dynamic relationship between the output force and velocity is guaranteed, and the contact force remains close to the allowable range.

2 System modeling

The schematic of the electro-hydraulic system is shown in Fig. 1. A drive cylinder attached to a mass load is controlled by a servo valve. A load cylinder, controlled by a servo valve, is used as the load. The goal is to make the mass load track the desired velocity trajectory as closely as possible when the load force lies in the allowable range. However, if the load force is beyond the desired range, an adjustment according to impedance rules needs to be made to keep an appropriate output force.

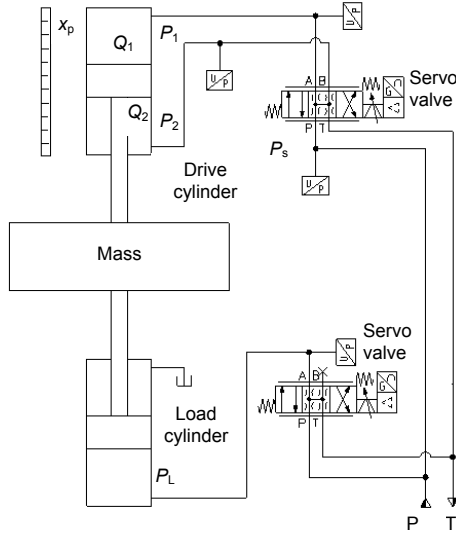


Fig. 1 Schematic of the electro-hydraulic system (P: high pressure oil; T: oil tank)

The drive cylinder, load cylinder, and mass load are fixed together (Fig. 1), and can be treated as a lumped mass load m . The dynamics of the lumped mass load can be described as

$$m\ddot{x}_p = P_1 A_1 - P_2 A_2 - b_1 \dot{x}_p - F_L + mg - F_{ic} - d, \quad (1)$$

where x_p is the displacement of the load mass, P_1 and P_2 are pressures of the drive cylinder forward and return chambers respectively, A_1 and A_2 are the ram

areas of the forward and return chambers respectively, g is gravitational acceleration, $F_{ic}(\dot{x}_p) = b_3 \tanh(\eta \dot{x}_p)$ is the modeled Coulomb friction force, d is the lumped uncertain nonlinearities due to external disturbances, unmodeled friction forces, and other hard-to-model terms, and F_L is the load force of the drive cylinder caused by the load cylinder, $F_L = b_2 s_g(\dot{x}_p) \dot{x}_p^2$, where $s_g(\cdot)$ will be defined later. The load cylinder is used here to imitate a load commonly found in practice, the load force of which is relevant to the drive velocity. Besides, b_1 is the damping coefficient, b_2 is the coefficient of the load force, and b_3 and η are coefficients of the modeled Coulomb friction force.

Neglecting the external leakage, the pressure dynamics in drive cylinder chambers can be expressed as

$$\dot{P}_1 = \frac{\beta_e}{V_{01} + A_1 x_p} [Q_1 - A_1 \dot{x}_p - C_t (P_1 - P_2)], \quad (2)$$

$$\dot{P}_2 = \frac{\beta_e}{V_{02} - A_2 x_p} [-Q_2 + A_2 \dot{x}_p + C_t (P_1 - P_2)], \quad (3)$$

where V_{01} and V_{02} are initial control volumes of the two drive cylinder chambers respectively, β_e is the effective hydraulic fluid bulk modulus, C_t is the coefficient of the total internal leakage of the cylinder due to pressure, Q_1 is the supply flow rate to the forward chamber, and Q_2 is the return flow rate out of the return chamber.

The control flow of the drive cylinder chambers Q_1 and Q_2 can be described as

$$Q_1 = k_q x_v [s_g(x_v) \sqrt{P_s - P_1} + s_g(-x_v) \sqrt{P_1 - P_t}], \quad (4)$$

$$Q_2 = k_q x_v [s_g(x_v) \sqrt{P_2 - P_t} + s_g(-x_v) \sqrt{P_s - P_2}], \quad (5)$$

where k_q is the flow gain coefficient of the servo valves, x_v is the spool displacement of the servo valves, P_s is the supply pressure of the pump, and P_t is the tank pressure. $s_g(\cdot)$ is defined as

$$s_g(\cdot) = \begin{cases} 1, & \text{if } \cdot \geq 0, \\ 0, & \text{if } \cdot < 0. \end{cases} \quad (6)$$

The dynamics of servo valves can be neglected,

because high-response servo valves are used here. Therefore, it is assumed that the control voltage applied to the servo valves is proportional to the spool position, that is, $x_v = k_x u$, where k_x is a positive constant and u is the control input voltage. For simplicity, define $k_{qx} = k_q k_x$.

Combining Eqs. (1)–(6) and defining $\mathbf{x} = [x_1, x_2, x_3, x_4]^T = [x_p, \dot{x}_p, P_1, P_2]^T$ as the state variable, the dynamics of the electro-hydraulic actuator in the state space can be expressed as

$$\dot{x}_1 = x_2, \quad (7)$$

$$\dot{x}_2 = \frac{1}{m} (A_1 x_3 - A_2 x_4 - b_1 x_2 - F_L + mg - F_{fc} - d), \quad (8)$$

$$\dot{x}_3 = h_1(x_1) [-A_1 x_2 - C_t(x_3 - x_4) + k_{qx} u g_1(x_3, u)], \quad (9)$$

$$\dot{x}_4 = h_2(x_1) [A_2 x_2 + C_t(x_3 - x_4) - k_{qx} u g_2(x_4, u)], \quad (10)$$

where

$$h_1(x) = \frac{\beta_e}{V_{01} + A_1 x_1}, \quad (11)$$

$$h_2(x) = \frac{\beta_e}{V_{02} - A_2 x_1}, \quad (12)$$

$$g_1(x_3, u) = s_g(u) \sqrt{P_s - x_3} + s_g(-u) \sqrt{x_3 - P_t}, \quad (13)$$

$$g_2(x_4, u) = s_g(u) \sqrt{x_4 - P_t} + s_g(-u) \sqrt{P_s - x_4}. \quad (14)$$

A new state variable is introduced as $\bar{x}_3 = x_3 - \alpha x_4$, where $\alpha = A_2/A_1$ represents the piston area ratio. Thus, the system of Eqs. (7)–(10) can be handled well using the backstepping technique. So, the dynamics of the whole system can be expressed as

$$\dot{x}_1 = x_2, \quad (15)$$

$$\dot{x}_2 = \frac{1}{m} [A_1 \bar{x}_3 - b_1 x_2 - b_2 s_g(x_2) x_2^2 + mg - b_3 \tanh(\eta x_2) - d], \quad (16)$$

$$\dot{\bar{x}}_3 = -f_1 x_2 - f_2 C_t(x_3 - x_4) + k_{qx} f_3 u, \quad (17)$$

where

$$f_1(x_1) = h_1(x_1) A_1 + \alpha h_2(x_1) A_2, \quad (18)$$

$$f_2(x_1) = h_1(x_1) + \alpha h_2(x_1), \quad (19)$$

$$f_3(x_1, x_3, x_4, u) = h_1(x_1) g_1(u, x_3) + \alpha h_2(x_1) g_2(u, x_4). \quad (20)$$

Before describing the controller design, we make the following assumption:

Assumption 1 The desired velocity trajectory \dot{x}_d and the derivatives \ddot{x}_d are bounded. P_1 and P_2 are bounded by P_s and P_t , respectively; that is, $0 \leq P_1 < P_1 < P_s$, $0 \leq P_2 < P_2 < P_s$.

3 Fuzzy impedance control

The load force F_L should be maintained in a certain allowable range to protect the environment or workpieces. As working conditions are always time-variant in practice, fuzzy impedance control is adopted to obtain a prescribed dynamic behavior between velocity control and force control. The impedance rule is defined as a first-order system:

$$m_c \ddot{e}_x + b_c \dot{e}_x = e_F, \quad (21)$$

where m_c is the desired mass and b_c is the desired damping coefficient. $e_F = F_L - F_{Ld}$ is the force discrepancy between the actual load force F_L and the desired load force F_{Ld} , $\dot{e}_x = \dot{x}_d - \dot{x}_1$ is the output velocity discrepancy, and \ddot{e}_x is its derivative.

Because of the variation in the velocity command and the load force requirement, it is necessary to define a number of impedance rules to regulate the dynamic behavior between velocity and load force. Thus, a fuzzy algorithm is employed to regulate impedance rules.

A Mamdani type of fuzzy inference engine and the center of gravity defuzzification methods are chosen to calculate the fuzzy controller. Seven membership functions, namely LS, CS, S, M, B, CB, and LB, are used for the input variables V_c and $|dF_c/dt|$ in a range of 0–1 (Fig. 2). Seven membership functions, namely NB, NM, NS, ZO, PS, PM, and PB, are used for the input variable dF_c in a range of –1–1 (Fig. 3). Seven membership functions, namely LS, CS, S, M, B, CB, and LB, are used for the output variable M in a range of 0–1 (Fig. 4). As for the output variable B , eight membership functions, namely LS, CS, S, SS, SB, B, CB, and LB, are used in a range of 0–1 (Fig. 5). Scaling functions should be used to regulate variables within the desired range, expressed as

$$V_c = \frac{1}{2} + \frac{1}{v_{\max} - v_{\min}} \left(v_c - \frac{v_{\max} + v_{\min}}{2} \right), \quad (22)$$

$$\left| \frac{dF_c}{dt} \right| = \frac{1}{2} + \frac{1}{|dF_L/dt|_{\max} - |dF_L/dt|_{\min}} \cdot \left(\left| \frac{dF_L}{dt} \right| - \frac{|dF_L/dt|_{\max} + |dF_L/dt|_{\min}}{2} \right), \quad (23)$$

$$dF_c = dF_L / dF_{L, \max}, \quad (24)$$

$$m_c = (m_{c, \max} - m_{c, \min})M + m_{c, \min}, \quad (25)$$

$$b_c = (b_{c, \max} - b_{c, \min})B + b_{c, \min}, \quad (26)$$

where $v_c = \dot{x}_d$ is the velocity command, v_{\max} and v_{\min} are its maximum and minimum respectively, $|dF_L/dt|_{\max}$ and $|dF_L/dt|_{\min}$ are the maximum and minimum absolute values of the derivative of F_L respectively, and $dF_{L, \max}$ is the maximum of the discrepancy between the actual load force and the nominal load force. The nominal load force is the force generated by the load cylinder when it moves at a desired velocity with a normal load. In practice, the nominal load force can be measured in advance. $m_{c, \max}$ and $m_{c, \min}$ are the maximum and minimum of the desired mass respectively, and $b_{c, \max}$ and $b_{c, \min}$ are the maximum and minimum of the desired damping coefficients respectively.

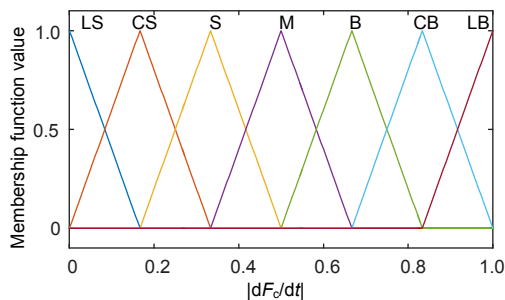


Fig. 2 Membership functions for the inputs V_c and $|dF_c/dt|$

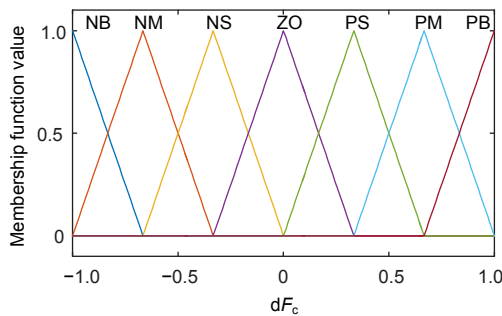


Fig. 3 Membership functions for the input dF_c

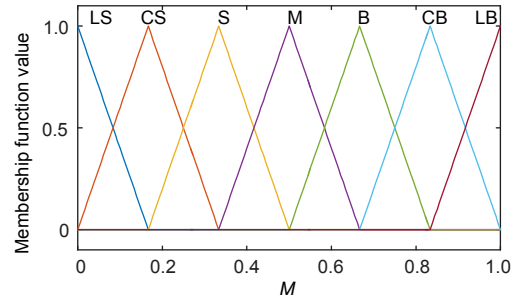


Fig. 4 Membership functions for the output M

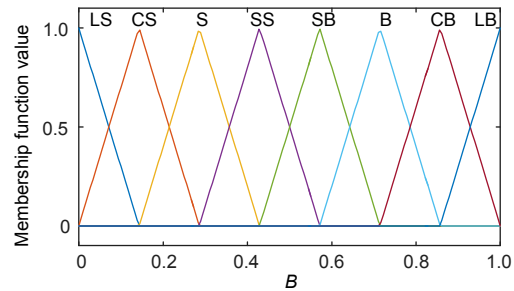


Fig. 5 Membership functions for the output B

The fuzzy rules are listed in Tables 1 and 2. The input variables are the velocity command V_c , the load force discrepancy dF_c , and the absolute value of its derivative $|dF_c/dt|$. The output variables are the desired mass M and the desired damping coefficient B of the impedance rules.

Table 1 Fuzzy rules of the desired mass M

$ dF_c/dt $	M						
	$V_c=LS$	CS	S	M	B	CB	LB
LS	LB	LB	CB	CB	B	B	M
CS	LB	CB	CB	B	B	M	S
S	CB	CB	B	B	M	S	S
M	CB	B	B	M	S	S	CS
B	B	B	M	S	S	CS	CS
CB	B	M	S	S	CS	CS	LS
LB	M	S	S	CS	CS	LS	LS

Table 2 Fuzzy rules of the desired damping coefficient B

dF_c	B						
	$V_c=LS$	CS	S	M	B	CB	LB
NB	B	SB	SS	S	CS	LS	LS
NM	CB	B	SB	SS	S	CS	LS
NS	LB	CB	B	SB	SS	S	CS
ZO	LB	LB	CB	B	SB	SS	S
PS	LB	CB	B	SB	SS	S	CS
PM	CB	B	SB	SS	S	CS	LS
PB	B	SB	SS	S	CS	LS	LS

Taking fuzzy impedance control into consideration, the desired velocity trajectory becomes $\dot{x}_s = \dot{x}_d - \dot{\tilde{e}}_x$ and the derivative becomes $\ddot{x}_s = \ddot{x}_d - \ddot{\tilde{e}}_x$, where $\dot{\tilde{e}}_x$ and $\ddot{\tilde{e}}_x$ are the computations of Eq. (21), which are different from \dot{e}_x and \ddot{e}_x .

Assumption 2 According to Assumption 1, assume that the first-order impedance strategy and the concerned load system, i.e., \dot{x}_s and \ddot{x}_s respectively, are bounded.

4 Extended disturbance observer based nonlinear velocity controller

4.1 Extended disturbance observer

The electro-hydraulic system is subjected to the external disturbances and parameter uncertainties, which will diminish control precision. An extended disturbance observer is proposed, driven by not only the control error but also the estimation error of state x_2 . In practice, x_2 can be measured with sensors. The dynamics estimation of x_2 is

$$\dot{\hat{x}}_{2p} = \frac{1}{m} \left[A_1 \bar{x}_3 - \hat{b}_1 x_2 - \hat{b}_2 s_g(x_2) x_2^2 + mg - \hat{b}_3 \tan h(\eta x_2) - \hat{d} + w_1 \tilde{x}_{2p} \right], \tag{27}$$

where \hat{x}_{2p} , \hat{b}_1 , \hat{b}_2 , \hat{b}_3 , and \hat{d} are estimations of x_2 , b_1 , b_2 , b_3 , and d respectively, and w_1 is a positive constant. The estimation errors are defined as $\tilde{x}_{2p} = x_2 - \hat{x}_{2p}$, $\tilde{b}_1 = b_1 - \hat{b}_1$, $\tilde{b}_2 = b_2 - \hat{b}_2$, $\tilde{b}_3 = b_3 - \hat{b}_3$, $\tilde{d} = d - \hat{d}$. Thus, the dynamics of \tilde{x}_{2p} is

$$\dot{\tilde{x}}_{2p} = -\frac{1}{m} \left[\tilde{b}_1 x_2 + \tilde{b}_2 s_g(x_2) x_2^2 + \tilde{b}_3 \tan h(\eta x_2) + \tilde{d} + w_1 \tilde{x}_{2p} \right]. \tag{28}$$

Adaption laws are chosen as

$$\dot{\hat{b}}_1 = -k_{11} \frac{1}{m} x_2 \tilde{x}_{2p} + \chi_{b1}, \tag{29}$$

$$\dot{\hat{b}}_2 = -k_{12} \frac{1}{m} s_g(x_2) x_2^2 \tilde{x}_{2p} + \chi_{b2}, \tag{30}$$

$$\dot{\hat{b}}_3 = -k_{13} \frac{1}{m} \tan h(\eta x_2) \tilde{x}_{2p} + \chi_{b3}, \tag{31}$$

$$\dot{\hat{d}} = -k_{14} \frac{1}{m} \tilde{x}_{2p} + \chi_d, \tag{32}$$

where k_{11} , k_{12} , k_{13} , and k_{14} are positive constants, and χ_{b1} , χ_{b2} , χ_{b3} , and χ_d are extra corrector terms, which will be designed later, to ensure the stability of the nonlinear velocity control system based on an extended disturbance observer.

Define the Lyapunov function as

$$V_1 = \frac{1}{2} \tilde{x}_{2p}^2 + \frac{1}{2} k_{11}^{-1} \tilde{b}_1^2 + \frac{1}{2} k_{12}^{-1} \tilde{b}_2^2 + \frac{1}{2} k_{13}^{-1} \tilde{b}_3^2 + \frac{1}{2} k_{14}^{-1} \tilde{d}^2. \tag{33}$$

Based on Eqs. (28)–(32), the time derivative of V_1 is

$$\dot{V}_1 = -\frac{1}{m} w_1 \tilde{x}_{2p}^2 - k_{11}^{-1} \tilde{b}_1 \chi_{b1} - k_{12}^{-1} \tilde{b}_2 \chi_{b2} - k_{13}^{-1} \tilde{b}_3 \chi_{b3} - k_{14}^{-1} \tilde{d} \chi_d. \tag{34}$$

Remark 1 The dynamics of b_1 , b_2 , b_3 , and d are ignored and treated as constant. However, it can be proved by experiments that the proposed controller is reliable in practice with the time-variant parameters b_1 , b_2 , b_3 , and disturbance d .

4.2 Nonlinear velocity controller

The velocity controller is designed based on a recursive backstepping procedure, consisting of a velocity tracking outer loop and a pressure control inner loop.

1. Step 1

Define the velocity tracking error as $\tilde{x}_2 = x_2 - \dot{x}_s$. Then a sliding surface s can be defined as

$$s = \tilde{x}_2 + \lambda \int \tilde{x}_2 dt, \tag{35}$$

where λ is a positive constant. Since making \tilde{x}_2 small or converge to zero is equivalent to making s small or converge to zero, the rest of the design will focus on making s as small as possible. According to Assumption 2, differentiating Eq. (35) and noting Eqs. (15)–(17) yield

$$\dot{s} = \frac{1}{m} \left[A_1 \bar{x}_3 - b_1 x_2 - b_2 s_g(x_2) x_2^2 + mg - b_3 \tan h(\eta x_2) - d \right] - \ddot{x}_s + \lambda(x_2 - \dot{x}_s). \tag{36}$$

A virtual control input $\bar{\alpha}_3$ for \bar{x}_3 is designed as

$$\bar{\alpha}_3 = \frac{1}{A_1} \left[\hat{b}_1 x_2 + \hat{b}_2 s_g(x_2) x_2^2 - mg + \hat{b}_3 \tanh(\eta x_2) + \hat{d} + m(\ddot{x}_s - \lambda(x_2 - \dot{x}_s) - c_1 s) \right] \quad (37)$$

where c_1 is a positive constant.

Let $\bar{z}_3 = \bar{x}_3 - \bar{\alpha}_3$ denote the inner pressure control loop error. The dynamics of s can be expressed as

$$\dot{s} = -c_1 s + \frac{A_1}{m} \bar{z}_3 - \frac{1}{m} \tilde{b}_1 x_2 - \frac{1}{m} \tilde{b}_2 s_g(x_2) x_2^2 - \frac{1}{m} \tilde{b}_3 \tanh(\eta x_2) - \frac{1}{m} \tilde{d} \quad (38)$$

Define the following Lyapunov function:

$$V_2 = V_1 + \frac{1}{2} k_2^{-1} s^2, \quad (39)$$

where k_2 is a positive constant. Taking Eqs. (34) and (38) into consideration, the time derivative of V_2 is given by

$$\begin{aligned} \dot{V}_2 = & -\frac{1}{m} w_1 x_{2p}^2 - k_{11}^{-1} \tilde{b}_1 \chi_{b1} - k_{12}^{-1} \tilde{b}_2 \chi_{b2} - k_{13}^{-1} \tilde{b}_3 \chi_{b3} \\ & - k_{14}^{-1} \tilde{d} \chi_d + k_2^{-1} s \left[-c_1 s + \frac{A_1}{m} z_3 - \frac{1}{m} \tilde{b}_1 x_2 \right. \\ & \left. - \frac{1}{m} \tilde{b}_2 s_g(x_2) x_2^2 - \frac{1}{m} \tilde{b}_3 \tanh(\eta x_2) - \frac{1}{m} \tilde{d} \right]. \end{aligned} \quad (40)$$

According to Eq. (40), the extra corrector terms χ_{b1} , χ_{b2} , χ_{b3} , and χ_d are designed as

$$\chi_{b1} = -\frac{1}{m} k_{11} k_2^{-1} x_2 s, \quad (41)$$

$$\chi_{b2} = -\frac{1}{m} k_{12} k_2^{-1} s_g(x_2) x_2^2 s, \quad (42)$$

$$\chi_{b3} = -\frac{1}{m} k_{13} k_2^{-1} \tanh(\eta x_2) s, \quad (43)$$

$$\chi_d = -\frac{1}{m} k_{14} k_2^{-1} s. \quad (44)$$

Combining Eqs. (40)–(44) yields

$$\dot{V}_2 = -\frac{1}{m} w_1 \tilde{x}_{2p}^2 - c_1 k_2^{-1} s^2 + k_2^{-1} \frac{A_1}{m} \bar{z}_3 s. \quad (45)$$

2. Step 2

The time derivative of \bar{z}_3 is given by

$$\dot{\bar{z}}_3 = -f_1 x_2 - f_2 C_1(x_3 - x_4) + k_{qx} f_3 u - \dot{\bar{\alpha}}_3. \quad (46)$$

Thus, an actual control input u should be synthesized to guarantee that \bar{x}_3 tracks the virtual control input $\bar{\alpha}_3$ with a certain transient performance. Similar to step 1, u is designed as

$$u = \frac{1}{k_{qx} f_3} \left[f_1 x_2 + f_2 C_1(x_3 - x_4) + \dot{\bar{\alpha}}_3 - c_2 \bar{z}_3 - k_2^{-1} k_3 \frac{A_1}{m} s \right], \quad (47)$$

where c_2 and k_3 are positive constants.

Remark 2 Although Eq. (47) includes the control input u on both sides, u on the right side is only in the term $s_g(\cdot)$ of f_3 . As f_3 and k_{qx} are always larger than zero, u is determined by only $f_1 x_2 + f_2 C_1(x_3 - x_4) + \dot{\bar{\alpha}}_3 - c_2 \bar{z}_3 - k_2^{-1} k_3 A_1 s / m$.

Hence, the control input u can be modified as

$$u = \frac{u_b}{k_{qx} f_3(x_1, x_3, x_4, u_b)}, \quad (48)$$

$$u_b = f_1 x_2 + f_2 C_1(x_3 - x_4) + \dot{\bar{\alpha}}_3 - c_2 \bar{z}_3 - k_2^{-1} k_3 \frac{A_1}{m} s. \quad (49)$$

5 Stability analysis of the whole system

The whole cascade system consists of a fuzzy impedance controller and an extended disturbance based nonlinear velocity controller (Fig. 6). Parameters of the impedance rules are determined by a fuzzy algorithm. The impedance system defined as Eq. (21) is a time-variant first-order system with positive coefficients, while the input e_F is limited by the specific load system. So, the defined first-order system is always stable, and the time-variant parameters change only the settling time and output value.

Define a sliding function as

$$s_1 = m_c \ddot{e}_x + b_c \dot{e}_x - e_F. \quad (50)$$

The sliding function of Eq. (50) produces the desired impedance behavior of Eq. (21), if s_1 vanishes

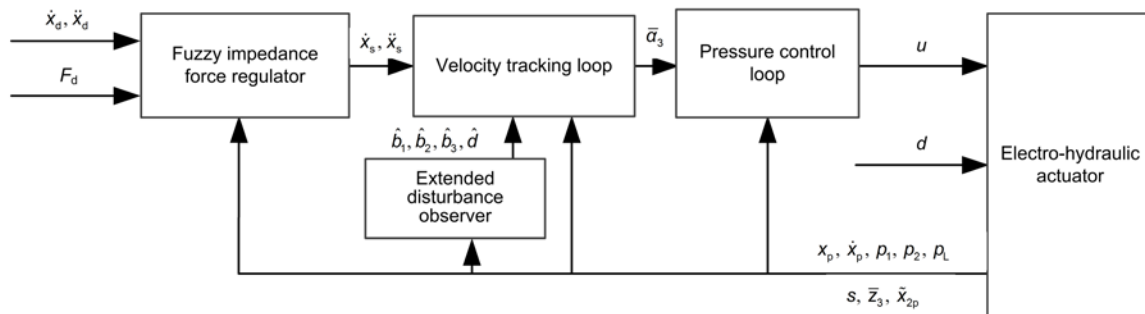


Fig. 6 Block diagram of the whole system

(Xu, 2015). Then Eq. (50) yields

$$\begin{aligned}
 s_1 &= m_c(\ddot{x}_d - \ddot{x}_1) + b_c(\dot{x}_d - \dot{x}_1) - e_f \\
 &= m_c(\ddot{\tilde{e}}_x - \ddot{\tilde{x}}_2) + b_c(\dot{\tilde{e}}_x - \dot{\tilde{x}}_2) - e_f \quad (51) \\
 &= -(m_c\ddot{\tilde{x}}_2 + b_c\dot{\tilde{x}}_2).
 \end{aligned}$$

The stability of EDOBC can be proved by substituting Eq. (47) into Eq. (46). \bar{z}_3 can be expressed as

$$\dot{\bar{z}}_3 = -c_2\bar{z}_3 - k_2^{-1}k_3 \frac{A_1}{m}s. \quad (52)$$

Define the following Lyapunov function:

$$V_3 = V_2 + \frac{1}{2}k_3^{-1}\bar{z}_3^2. \quad (53)$$

Taking Eqs. (45), (52), and (53) into consideration, the time derivative of V_3 is given by

$$\dot{V}_3 = -\frac{1}{m}w_1\tilde{x}_{2p}^2 - c_1k_2^{-1}s^2 - c_2k_3^{-1}\bar{z}_3^2 \leq 0. \quad (54)$$

Therefore, the stability of EDOBC is proved. \tilde{x}_2 will converge to zero in finite time. Generally, the response of EDOBC is designed to be much faster than the fuzzy impedance controller, to keep the contact force varying smoothly and avoiding impacts. \dot{x}_s can be treated as zero when \ddot{x}_d is zero and the load varies slowly. So, $\dot{\tilde{x}}_2 = \dot{x}_2 - \dot{x}_s$ can be assumed to be small enough to make s_1 converge to zero. Therefore, the desired impedance behavior can be achieved under certain conditions.

6 Experimental results

Experiments were conducted to verify the performance of the proposed FICEDOB. A drive cylinder with an 80-mm bore and a 50-mm rod was controlled by a servo valve manufactured by Bosch (4WRREH6VB40L-1X/G24K0/B5M). The load cylinder had a 70-mm bore and a 50-mm rod controlled by another servo valve of the same type. The bandwidth of the servo valves was greater than 80 Hz with a 100% control signal. Four pressure sensors were installed, which were all made by Bosch Rexroth (HM20-1X400-C-K35) with an accuracy of 2×10^5 Pa. A position sensor made by SPM was used to measure the displacement of the drive cylinder. The velocity was obtained by differentiating the position signal. All these signals were fed back to, or output from a data acquisition card (National Instruments PCI-6229). The control algorithm was implemented in the Matlab Simulink Realtime environment with a control rate of 1 kHz.

The performance of EDOBC without impedance control was verified first. Parameters of the electro-hydraulic system and controllers are listed in Tables 3 and 4, respectively. The desired velocity trajectory was $\dot{x}_d = 0.02 \sin\left(\frac{\pi}{5}t + \frac{3\pi}{2}\right) + 0.03$ m/s, and the command of the servo valves controlling the load cylinder was $u_L = -2$ V. Figs. 7 and 8 show that the tracking errors are small. The control input u of EDOBC is shown in Fig. 9, and estimations of the parameters $\hat{b}_1, \hat{b}_2, \hat{b}_3$, and \hat{d} in Fig. 10. EDOBC had a good velocity tracking performance since the extended disturbance observer could compensate for external disturbances and parameter uncertainties

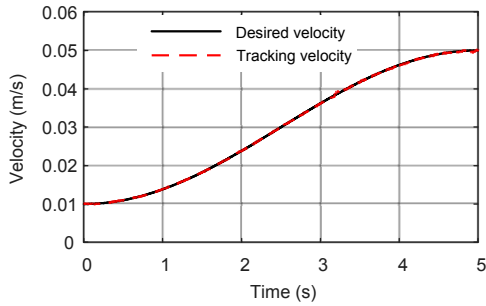


Fig. 7 Velocity tracking of the extended disturbance observer based nonlinear velocity control

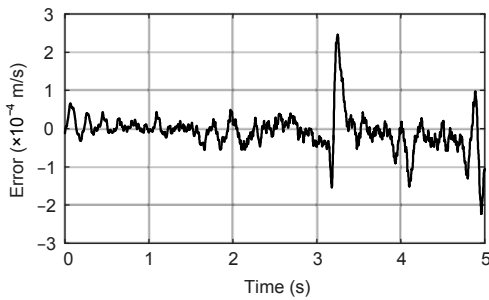


Fig. 8 Tracking errors of the extended disturbance observer based nonlinear velocity control

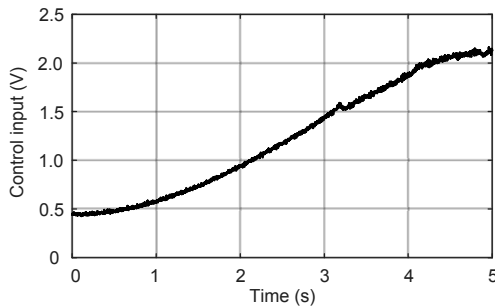


Fig. 9 Control input of the extended disturbance observer based nonlinear velocity control

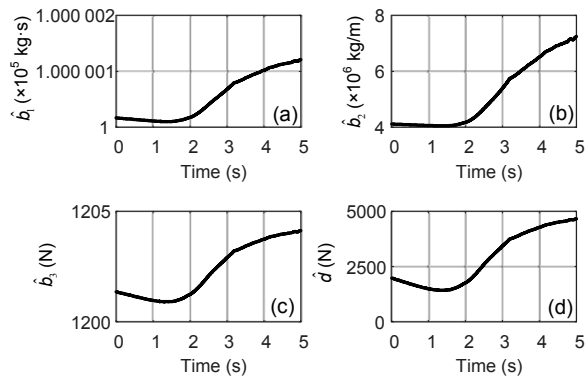


Fig. 10 Parameter estimations of the extended disturbance observer based nonlinear velocity control: (a) estimation of \hat{b}_1 ; (b) estimation of \hat{b}_2 ; (c) estimation of \hat{b}_3 ; (d) estimation of \hat{d}

during the tracking process. The initial estimations of parameters were defined based on parameter identification when $\dot{x}_d = 0.02$ m/s. The parameter estimations in Fig. 10 are consistent with the positive correlations between the cylinder velocity and the load force in analytic prediction. However, there is no guarantee that the estimated parameters are equal to their true values. This is because the parameter adaptation law is driven by both the control error and the estimation error of state x_2 , and the persistent excitation condition (Slotine and Li, 1991) may not be satisfied. However, high-performance velocity tracking and state observation can still be achieved through accurate force compensation, which is a combination of $\hat{b}_1 x_2$, $\hat{b}_2 s_g(x_2)x_2^2$, $\hat{b}_3 \tanh(\eta x_2)$, and \hat{d} . Once the control error and the state estimation error converge to zero, the estimated parameters become stable, but may not be equal to their true values.

Table 3 Parameters of the electro-hydraulic system

Symbol	Value	Unit
m	175	kg
A_1	5.0265×10^{-3}	m^2
A_2	3.0631×10^{-3}	m^2
η	100	s/m
g	9.8	m/s^2
P_s	2.100×10^7	Pa
P_t	0	Pa
C_t	0	$m^3/(s \cdot Pa)$
k_{qx}	3.5635×10^{-3}	$m^3/(s \cdot V \cdot \sqrt{Pa})$

Table 4 Parameters of the extended disturbance observer based nonlinear velocity control

Symbol	Value	Unit	Symbol	Value	Unit
k_{11}	1×10^5		λ	50	
k_{12}	8×10^{13}		c_1	1×10^4	
k_{13}	1×10^5		c_2	60	
k_{14}	1×10^8		$\hat{b}_1(0)$	1×10^5	kg-s
k_2	0.5		$\hat{b}_2(0)$	4×10^6	kg/m
k_3	1×10^5		$\hat{b}_3(0)$	1200	N
w_1	3×10^5		$\hat{d}(0)$	0	N

Next, FICEDOB was tested when the velocity commands were constant, set as 0.02 and 0.04 m/s. Parameters of the fuzzy impedance rules are listed in

Table 5. Two controllers, EDOBC and FICEDOB, were compared to verify the effect of impedance control. A sudden step-like change was applied to the servo valves that controlled the load cylinder. Due to limitations of EDOBC, the estimated parameters could not converge to their true values. Therefore, in practice, the load force was measured through a pressure sensor.

Table 5 Parameters of the fuzzy impedance rules

Symbol	Value	Unit	Symbol	Value	Unit
v_{\max}	0.05	m/s	$m_{c \max}$	1000	$\text{N}\cdot\text{s}^2/\text{m}$
v_{\min}	0	m/s	$m_{c \min}$	100	$\text{N}\cdot\text{s}^2/\text{m}$
$ dF_L/dt _{\max}$	1×10^5	N/s	$b_{c \max}$	4×10^6	$\text{N}\cdot\text{s}/\text{m}$
$ dF_L/dt _{\min}$	0	N/s	$b_{c \min}$	8×10^5	$\text{N}\cdot\text{s}/\text{m}$
$dF_{L \max}$	76970	N			

The velocity command was set as 0.02 m/s, and the load command changed from -1 V to -0.7 V and back to -1 V (step-like) (Fig. 11a). Fig. 11b shows the adjusted velocity command which helps achieve a desired impedance behavior when a change of load command occurs. Because of the fuzzy impedance control, a smooth and small velocity command was generated in FICEDOB. The load force on the load cylinder was kept within a close range (Fig. 11d). Tracking errors related to the unadjusted or adjusted velocity command are shown in Fig. 11c. Both FICEDOB and EDOBC achieved good tracking performance, while FICEDOB showed great robustness in dealing with load impacts by velocity adjustment.

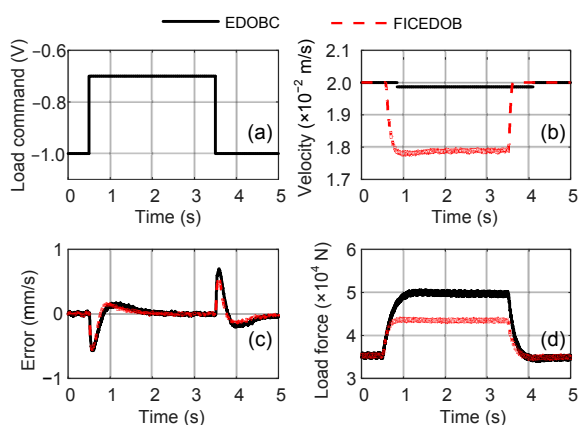


Fig. 11 Tracking results with a 0.02-m/s velocity command and $-1\rightarrow-0.7\rightarrow-1$ V load command: (a) load command; (b) adjusted velocity command; (c) velocity tracking error; (d) load force

In the experiments, fuzzy impedance control was activated if the discrepancy of the load force reached 10% beyond the nominal value. The experimental results showed that a balance of velocity control and force control could be easily achieved by tuning the relative values of the target impedance parameters. The fuzzy impedance parameter B was chosen smaller when the discrepancy of load force or velocity command became larger. A small load force error could be obtained if a small B or a small discrepancy which activated impedance was chosen, simultaneously leading to a large velocity error. However, acute oscillation could be excited when B or the discrepancy was too small (Xu, 2015). Hence, a fuzzy algorithm was adopted to determine the best target impedance parameters for specific applications.

To further test the effectiveness of the fuzzy impedance control strategy, different load commands and velocity commands were applied. No matter whether the load command became larger or smaller, FICEDOB showed both good force control ability and good velocity tracking performance. The test results are shown in Figs. 12–14. The velocity commands were set as 0.02 m/s in Fig. 12 and 0.04 m/s in Figs. 13 and 14. Similarly, a smoothly adjusted velocity command was produced when the load force reached the accepted range. The load force was kept in a narrower range with FICEDOB than with EDOBC. All experimental results indicated that FICEDOB can be employed in electro-hydraulic actuators to obtain a high-velocity tracking performance along with force regulation on the environment.

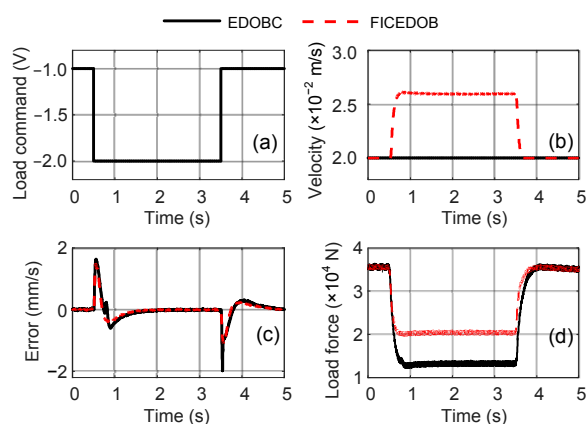


Fig. 12 Tracking results with a 0.02-m/s velocity command and $-1\rightarrow-2\rightarrow-1$ V load command: (a) load command; (b) adjusted velocity command; (c) velocity tracking error; (d) load force

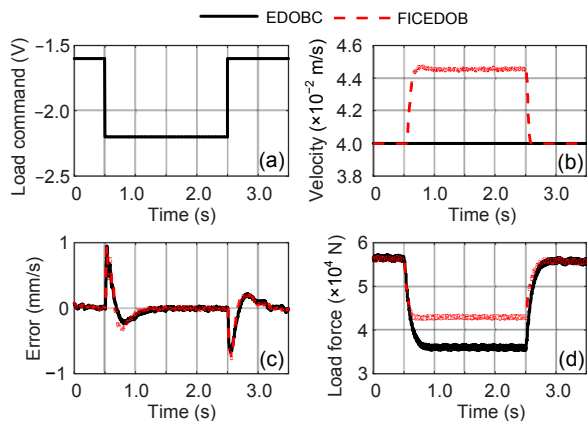


Fig. 13 Tracking results with a 0.04-m/s velocity command and $-1.6 \rightarrow -2.2 \rightarrow -1.6$ V load command: (a) load command; (b) adjusted velocity command; (c) velocity tracking error; (d) load force

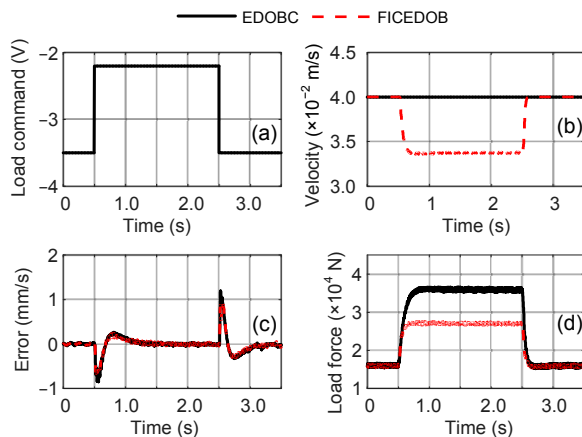


Fig. 14 Tracking results with a 0.04-m/s velocity command and $-3.5 \rightarrow -2.2 \rightarrow -3.5$ V load command: (a) load command; (b) adjusted velocity command; (c) velocity tracking error; (d) load force

The primary advantage of fuzzy impedance control is that it can regulate the dynamic relationship between velocity and force. Because the load force is caused by fluid flowing through an orifice, a stable load force will be established until the flow becomes stable. Therefore, the regulation of dynamics between velocity and force is not apparent in experiments; however, force adjustment performance is quite good.

To clearly demonstrate the force control ability of FICEDOB, velocity commands, stably adjusted velocity commands, and stable load forces are listed in Table 6. Fuzzy impedance control can regulate the load force within a narrow range, which can protect the environment.

It is obvious that velocity control and force control are coupled in the impedance control strategy (Xu, 2015). A desired velocity trajectory cannot be tracked arbitrarily without considering the force requirement in contact tasks. This limitation demands a compromise between velocity control and force control, which can be realized by a designed impedance scheme. In some applications, velocity control is considered the paramount goal, while the contact force is allowed to vary within some ranges. Using the proposed FICEDOB, it can be achieved by focusing more on velocity control than force control to obtain a better control performance.

7 Conclusions

In this study, an impedance control strategy has been combined with an extended disturbance observer based nonlinear velocity controller to deal with not only velocity control but also force control of an electro-hydraulic actuator. The proposed controller has combined the advantages of an impedance controller and an extended disturbance observer based nonlinear velocity controller. External disturbances and parameter uncertainties can be compensated for through EDOBC, while the regulation of velocity and force can be obtained via an impedance scheme. The parameters of the impedance controller have been adjusted by a fuzzy algorithm to achieve good performance. The fuzzy impedance controller has regulated the velocity command, which is the control target of EDOBC. Then accurate velocity control has been guaranteed by EDOBC. The stability of the whole cascade system has been analyzed. In experiments, high velocity tracking performance and force adjustment performance have been achieved, along with the successful cancelation of parameter uncertainties and disturbances, which verified the effectiveness of the proposed control strategy. Because the extended disturbance observer is driven by both the state estimation error and the tracking error once the errors converge to zero, the estimated parameters and disturbances are stable but may not trend towards their true values. In future work, we will consider the accurate estimation of load force rather than measuring it with a pressure sensor, such as using an indirect adaptive robust controller.

Compliance with ethics guidelines

Ming-jie LI, Jian-hua WEI, Jin-hui FANG, Wen-zhuo SHI, and Kai GUO declare that they have no conflict of interest.

References

- Ahn KK, Nam DNC, Jin ML, 2014. Adaptive backstepping control of an electrohydraulic actuator. *IEEE/ASME Trans Mech*, 19(3):987-995. <https://doi.org/10.1109/Tmech.2013.2265312>
- Chen WH, 2004. Disturbance observer based control for nonlinear systems. *IEEE/ASME Trans Mech*, 9(4):706-710. <https://doi.org/10.1109/Tmech.2004.839034>
- Chen YY, Zhao J, Wang BD, et al., 2005. High precision fuzzy impedance control of free-form surfaces polishing robotic arm based on position control. *Proc IEEE/ASME Int Conf on Advanced Intelligent Mechatronics*, p.819-824. <https://doi.org/10.1109/AIM.2005.1511084>
- Chen Z, Yao B, Wang QF, 2013. Accurate motion control of linear motors with adaptive robust compensation of nonlinear electromagnetic field effect. *IEEE/ASME Trans Mech*, 18(3):1122-1129. <https://doi.org/10.1109/Tmech.2012.2197217>
- Cui RX, Chen LP, Yang CG, et al., 2017. Extended state observer-based integral sliding mode control for an underwater robot with unknown disturbances and uncertain nonlinearities. *IEEE Trans Ind Electron*, 64(8):6785-6795. <https://doi.org/10.1109/Tie.2017.2694410>
- Fateh MM, 2010. Robust impedance control of a hydraulic suspension system. *Int J Robust Nonl*, 20(8):858-872. <https://doi.org/10.1002/rnc.1473>
- Fateh MM, Alavi SS, 2009. Impedance control of an active suspension system. *Mechatronics*, 19(1):134-140. <https://doi.org/10.1016/j.mechatronics.2008.05.005>
- Friedland B, Park YJ, 1992. On adaptive friction compensation. *IEEE Trans Autom Contr*, 37(10):1609-1612. <https://doi.org/10.1109/9.256395>
- Guo K, Wei JH, Fang JH, et al., 2015. Position tracking control of electro-hydraulic single-rod actuator based on an extended disturbance observer. *Mechatronics*, 27:47-56. <https://doi.org/10.1016/j.mechatronics.2015.02.003>
- Hogan N, 1985a. Impedance control: an approach to manipulation: part I—theory. *J Dynam Syst Meas Contr*, 107(1):1-7. <https://doi.org/10.1115/1.3140702>
- Hogan N, 1985b. Impedance control: an approach to manipulation: part II—implementation. *J Dynam Syst Meas Contr*, 107(1):8-16. <https://doi.org/10.1115/1.3140713>
- Hogan N, 1985c. Impedance control: an approach to manipulation: part III—applications. *J Dynam Syst Meas Contr*, 107(1):17-24. <https://doi.org/10.1115/1.3140701>
- Kim CS, Hong KS, Kim MK, 2005. Nonlinear robust control of a hydraulic elevator: experiment-based modeling and two-stage Lyapunov redesign. *Contr Eng Pract*, 13(6):789-803. <https://doi.org/10.1016/j.conengprac.2004.09.003>
- Kim W, Shin D, Won D, et al., 2013. Disturbance-observer-based position tracking controller in the presence of biased sinusoidal disturbance for electrohydraulic actuators. *IEEE Trans Contr Syst Technol*, 21(6):2290-2298. <https://doi.org/10.1109/TCST.2013.2237909>
- Li SZ, Wei JH, Guo K, et al., 2017. Nonlinear robust prediction control of hybrid active-passive heave compensator with extended disturbance observer. *IEEE Trans Ind Electron*, 64(8):6684-6694. <https://doi.org/10.1109/Tie.2017.2698358>
- Li ZJ, Liu JQ, Huang ZC, et al., 2017. Adaptive impedance control of human-robot cooperation using reinforcement learning. *IEEE Trans Ind Electron*, 64(10):8013-8022. <https://doi.org/10.1109/Tie.2017.2694391>
- Lin Y, Shi Y, Burton R, 2013. Modeling and robust discrete-time sliding-mode control design for a fluid power electrohydraulic actuator (EHA) system. *IEEE/ASME Trans Mech*, 18(1):1-10. <https://doi.org/10.1109/Tmech.2011.2160959>
- Mintsa HA, Venugopal R, Kenne JP, et al., 2012. Feedback linearization-based position control of an electrohydraulic servo system with supply pressure uncertainty. *IEEE Trans Contr Syst Technol*, 20(4):1092-1099. <https://doi.org/10.1109/Tcst.2011.2158101>
- Nam Y, 2001. QFT force loop design for the aerodynamic load simulator. *IEEE Trans Aerosp Electron Syst*, 37(4):1384-1392. <https://doi.org/10.1109/7.976973>
- Pi YJ, Wang XY, 2010. Observer-based cascade control of a 6-DOF parallel hydraulic manipulator in joint space coordinate. *Mechatronics*, 20(6):648-655. <https://doi.org/10.1016/j.mechatronics.2010.07.002>
- Raibert MH, Craig JJ, 1981. Hybrid position/force control of manipulators. *J Dynam Syst Meas Contr*, 103(2):126-133. <https://doi.org/10.1115/1.3139652>
- Sha DH, Bajic VB, Yang HY, 2002. New model and sliding mode control of hydraulic elevator velocity tracking system. *Simul Pract Theory*, 9(6-8):365-385. [https://doi.org/10.1016/S1569-190x\(02\)00058-8](https://doi.org/10.1016/S1569-190x(02)00058-8)
- Shibata M, Murakami T, Ohnishi K, 1996. A unified approach to position and force control by fuzzy logic. *IEEE Trans Ind Electron*, 43(1):81-87. <https://doi.org/10.1109/41.481411>
- Sirouspour MR, Salcudean SE, 2001. Nonlinear control of hydraulic robots. *IEEE Trans Rob Autom*, 17(2):173-182. <https://doi.org/10.1109/70.928562>
- Slotine JJE, Li W, 1991. *Applied Nonlinear Control*. Englewood Cliffs, New Jersey, Prentice Hall, USA.
- Tian QY, Wei JH, Fang JH, et al., 2016. Adaptive fuzzy integral sliding mode velocity control for the cutting system of a trench cutter. *Front Inform Technol Electron Eng*, 17(1):55-66. <https://doi.org/10.1631/FITEE.15a0160>
- Truong DQ, Ahn KK, 2009. Force control for hydraulic load simulator using self-tuning grey predictor-fuzzy PID. *Mechatronics*, 19(2):233-246. <https://doi.org/10.1016/j.mechatronics.2008.07.007>

- Wei JH, Zhang Q, Li MJ, et al., 2016. High-performance motion control of the hydraulic press based on an extended fuzzy disturbance observer. *Proc Inst Mech Eng Part I—J Syst Contr Eng*, 230(9):1044-1061. <https://doi.org/10.1177/0959651816662562>
- Xu GZ, Song AG, Li HJ, 2011. Adaptive impedance control for upper-limb rehabilitation robot using evolutionary dynamic recurrent fuzzy neural network. *J Intell Robot Syst*, 62(3-4):501-525. <https://doi.org/10.1007/s10846-010-9462-3>
- Xu QS, 2015. Robust impedance control of a compliant microgripper for high-speed position/force regulation. *IEEE Trans Ind Electron*, 62(2):1201-1209. <https://doi.org/10.1109/TIE.2014.2352605>
- Yang HY, Shi H, Gong GF, et al., 2009. Electro-hydraulic proportional control of thrust system for shield tunneling machine. *Autom Constr*, 18(7):950-956. <https://doi.org/10.1016/j.autcon.2009.04.005>
- Yao B, Tomizuka M, 1997. Adaptive robust control of SISO nonlinear systems in a semi-strict feedback form. *Automatica*, 33(5):893-900. [https://doi.org/10.1016/S0005-1098\(96\)00222-1](https://doi.org/10.1016/S0005-1098(96)00222-1)
- Yao B, Bu FP, Reedy J, et al., 2000. Adaptive robust motion control of single-rod hydraulic actuators: theory and experiments. *IEEE/ASME Trans Mech*, 5(1):79-91. <https://doi.org/10.1109/3516.828592>
- Yu L, Fei SM, Huang J, et al., 2017. Sliding mode switching control under arbitrary switchings in the presence of uncertain parameters. *Proc Inst Mech Eng Part I—J Syst Contr Eng*, 232(4):399-407. <https://doi.org/10.1177/0959651817709187>
- Zhang LB, Li ZJ, Yang CG, 2017. Adaptive neural network based variable stiffness control of uncertain robotic systems using disturbance observer. *IEEE Trans Ind Electron*, 64(3):2236-2245. <https://doi.org/10.1109/Tie.2016.2624260>
- Zhang Q, Fang JH, Wei JH, et al., 2016. Adaptive robust motion control of a fast forging hydraulic press considering the nonlinear uncertain accumulator model. *Proc Inst Mech Eng Part I—J Syst Contr Eng*, 230(6):483-497. <https://doi.org/10.1177/0959651816628994>
- Zhu WH, Piedboeuf JC, 2005. Adaptive output force tracking control of hydraulic cylinders with applications to robot manipulators. *J Dynam Syst Meas Contr*, 127(2):206-217. <https://doi.org/10.1115/1.1898237>